



Cite this: *J. Anal. At. Spectrom.*, 2022, **37**, 1738

# Direct analysis of nanoparticles in organic solvents by ICPMS with microdroplet injection†

Jovana Kocic, <sup>a</sup> Dmitry N. Dirin, <sup>ab</sup> Ralf Kägi, <sup>c</sup> Maksym V. Kovalenko, <sup>ab</sup> Detlef Günther <sup>a</sup> and Bodo Hattendorf <sup>\*,a</sup>

In recent years, the capabilities for characterizing inorganic nanoparticles (NPs) in aqueous solvents with respect to their elemental composition, mass and particle number concentration have been expanded using single particle inductively coupled plasma mass spectrometry (sp-ICPMS). However, NPs with high monodispersity, size, shape and surface chemistry control are frequently synthesized using hot-injection methods, utilizing hydrophobic organic ligands which are only soluble in non-polar organic solvents. Due to several instrumental limitations, suspensions in organic solvents are not commonly analysed by sp-ICPMS. In this study, we investigated the direct introduction of toluene and mesitylene into an ICPMS using a microdroplet generator. With this configuration the solvent load in the ICP is substantially reduced and soot formation, causing instrumental drift, was minimized while maintaining a transport efficiency (TE) of 100%. Furthermore, the effect of different vacuum interface configurations and the addition of oxygen or nitrogen on the detection efficiency (DE) and instrumental background signals was investigated for Al, Si, Ti, Fe, Cu, Ag, Cd, and Pb. The highest DE was obtained for a "Jet" interface with the addition of nitrogen at a flow rate of 10 mL min<sup>-1</sup>, resulting in an increase by a factor of 2–8 depending on the element. The lowest detectable mass, based on counting statistics, was 1.4 ag for Pb, which corresponds to a diameter of 6.1 nm of a spherical, metallic NP. The approach can not only be used for NP characterization, but also holds promise for the sensitive determination of trace elements in organic solvents.

Received 15th October 2021  
 Accepted 24th June 2022

DOI: 10.1039/d1ja00358e

[rsc.li/jaas](http://rsc.li/jaas)

## Introduction

Single-particle inductively coupled plasma mass spectrometry (sp-ICPMS) has become a frequently used technique for characterizing inorganic nanoparticles (NPs) as it can provide information about elemental mass content, the particle number concentration (PNC), and, if present, the dissolved fraction of an element.<sup>1,2</sup> In most previous studies however, sp-ICPMS was used to assess NPs present in aqueous suspensions. On the other hand, NPs are often synthesized and stabilized by bulky organic ligands and dissolved in non-polar organic solvents, such as toluene, mesitylene, hexane, chloroform, *etc.*<sup>3–9</sup> Because such solvents are usually difficult to analyse with ICPMS, direct analysis of NPs suspended in organic solvents using sp-ICPMS has rarely been discussed in the literature: Nelson *et al.*<sup>10,11</sup> studied iron- and molybdenum-containing NPs in *o*-xylene with sizes of 60–400 nm and 70 nm, respectively, while Ruhland *et al.*<sup>12</sup> investigated mercury-containing NPs with median size of

about 190 nm suspended in tetrahydrofuran (THF). The reason for the limited number of reports applying sp-ICPMS to non-aqueous solutions of NPs relates to various challenges associated with introducing organic solvents into an ICPMS. Leclercq *et al.*<sup>13,14</sup> reviewed the theoretical and practical aspects of analysing non-aqueous solutions with ICPMS and discussed the various drawbacks: when organic solvents are introduced into an ICPMS, soot can form and deposit at the torch, vacuum interface, and ion lenses<sup>13–15</sup> (see Fig. S1†). This can affect the long-term stability of the instrument and usually leads to signal suppression. Furthermore, additional molecular ions may be formed from the solvent, causing spectral interferences. To avoid these adverse effects, carbon is often combusted by adding oxygen to the aerosol stream. However, the use of oxygen for experiments with hydrocarbon solvents also has certain disadvantages, such as suppression of analyte sensitivity,<sup>16</sup> higher levels of O-based molecular ions and instrument wear, in particular when using a vacuum interface with Ni-cones.<sup>17</sup> In order to avoid the latter, the more expensive Pt cones<sup>13,18</sup> must be used instead. Crucial physicochemical parameters of organic solvents that influence plasma stability and ionization efficiency are volatility and dissociation energy which are typically higher than for water.<sup>19</sup> Therefore, at comparable sample flow rates, the attainable sensitivity for trace element determinations in organic solutions is lower. To overcome these drawbacks and

<sup>a</sup>Department of Chemistry and Applied Biosciences, ETH Zurich, Zurich, Switzerland.  
 E-mail: [bodo@inorg.chem.ethz.ch](mailto:bodo@inorg.chem.ethz.ch)

<sup>b</sup>Empa-Swiss Federal Laboratories for Materials Science and Technology, Dübendorf, Switzerland

<sup>c</sup>Department of Process Engineering, Eawag, Dübendorf, Switzerland

† Electronic supplementary information (ESI) available. See <https://doi.org/10.1039/d1ja00358e>



avoid the addition of oxygen to the ICP, different approaches have been suggested. Verboket *et al.*<sup>20</sup> described a method for introducing droplets containing an aqueous sample entrapped in perfluorohexane (PFH) into an ICPMS using a specially designed liquid-assisted droplet ejection chip. To reduce solvent loading, membrane desolvation was used to remove most of the PFH. In their study, the transport efficiency (TE) of approximately 50  $\mu\text{m}$  droplets was reported to be >50%.

Quantitative transfer of minute amounts of liquids into the ICP can be achieved using a microdroplet generator (MDG). Already in 1997, Lazar *et al.*<sup>17</sup> used monodisperse droplets of xylene for sample introduction into ICPOES. The use of an MDG for introduction of aqueous samples in sp-ICPMS analyses has been studied in detail for example by Koch *et al.*,<sup>21</sup> Gschwind *et al.*<sup>22,23</sup> and Shigeta *et al.*<sup>24</sup> The use of MDG-based setups has become very attractive for various studies of complex matrices. By reducing the sample uptake, matrix effects can be reduced, and the TE of the introduced solution can be improved. Recently, a dual sample introduction system, combining a conventional nebulization for the introduction of NP suspensions and an MDG for the addition of a calibration standard into the stream of nebulized solution into the ICP, is used to account for matrix effects and changes in the TE of the sample aerosol.<sup>2,25–27</sup> In addition, droplet-based introduction is used to characterize individual cells by ICPMS.<sup>20,28</sup> A low sample uptake rate is desirable in this regard as the available volume for analysis is often limited. Recently, Vonderach *et al.*<sup>29</sup> presented a downwards oriented ICPMS for the analysis of micro-samples, where droplet introduction *via* an MDG was successfully carried out at frequencies up to 1000 Hz.

Another advantage of MDG-based sample introduction is the tight control of the droplet volume, which enables the assessment of the absolute sensitivity of the ICPMS. Due to the limited availability of NP reference materials, determination of NP mass is frequently accomplished by calibrating the instrument using ionic standards with known elemental content. Droplets of known size and known element content on the other hand provide a unique means to establish a calibration in terms of absolute sensitivities in a highly flexible manner without the need to determine the transport efficiency by other means. Furthermore, by reducing the sample load into the plasma, soot formation can be mitigated when using organic solvents and oxygen addition may not be required for stable operation.

In a previous paper, the detection capabilities of ICPMS with “Jet” interface and nitrogen addition were studied for the analysis of NPs dispersed in aqueous suspensions.<sup>30</sup> With this setup, up to 1000 times higher detection efficiency (DE) could be achieved, while the mass discrimination of the instrument was significantly reduced. The size limit of detection (LOD) for NPs suspended in aqueous solution could be lowered to the single-digit nm range, even for materials such as  $\text{TiO}_2$  that otherwise showed a much poorer response.

In this work we aimed to characterize sample introduction using an MDG and a high-sensitivity ICPMS for the measurement of NPs dispersed in organic solvents. Toluene and mesitylene based droplets were introduced directly into the ICPMS and the figures of merit using the high sensitivity “Jet” interface

and the standard interface were compared. The influence of oxygen and nitrogen gas addition was investigated in order to optimize the DE of eight different elements and minimize the formation and impact of soot deposits and molecular ions from the solvent. Finally, analyses of previously characterized 80 nm Ag reference NPs, and  $\text{TiO}_2$  NPs from sunscreen lotions were performed. Samples were diluted directly in toluene, mixture of toluene and dodecanethiol, mesitylene and mixture of mesitylene and dodecanethiol. In order to compare size and particle number concentration of sunscreen lotion, sunscreen sample was directly diluted into water, following the evaluated sample preparation procedure used for interlaboratory comparisons.<sup>31</sup>

## Experimental section

### Materials and chemicals

Multi-element standard solutions were prepared from Conostan S-21 (21 elements, 10  $\text{mg L}^{-1}$  in 75 cSt oil, SCP Science, Canada) in toluene (extra dry over molecular sieve 99.85%, Acros Organics, Belgium) and mesitylene (Sigma-Aldrich, USA). To further investigate the stabilization of inorganic NPs in suspension, 10 mM dodecanethiol (DDT, Sigma-Aldrich, USA) was added to the organic solvents. Aqueous standards were prepared from stock solutions of Ti (1000  $\text{mg L}^{-1}$ , Alfa Aesar, Thermo Fisher Scientific, USA) and In (10  $\text{mg L}^{-1}$ , Inorganic Ventures, Christiansburg, Virginia, USA). The concentrations of the standard solutions were in the range of 1–50  $\mu\text{g kg}^{-1}$ . Ag NPs from a commercial citrate-stabilized suspension with a nominal size of  $78.9 \pm 3.9$  nm (NanoXact™ Silver, NanoComposix, San Diego, California, USA) were transferred into toluene by solvent and ligand exchange. A detailed procedure for the ligand exchange is given in the ESI.†

Sunscreen samples from different manufacturers were purchased at a local store. All samples were stored in a fridge and left to warm to room temperature for 30 minutes before further sample preparation. The suspensions were diluted gravimetrically using an electronic balance (dual scale reading of 0.01 mg/0.1 mg, Mettler XSR205DU, Mettler Toledo, Greifensee, Switzerland), and sonicated for 15 minutes before each dilution step (Bandelin Sonorex, Faust Laborbedarf AG, Schaffhausen, Switzerland).

All suspensions were sonicated immediately prior to the analyses. Conditioned 20 mL glass vials were used for the preparation of standards and samples solvents. The vials were cleaned by boiling in *aqua regia* for 30 minutes and then rinsing with ultra-pure water. The *aqua regia* was prepared from HCl (Optima Grade, Fisher Scientific, United Kingdom) and sub-boiled  $\text{HNO}_3$  prepared in our laboratory. After drying, they were filled with the respective solvents and conditioned overnight.

### Instrumentation and data acquisition

A sector-field ICPMS (Element XR, Thermo Scientific, Bremen, Germany) was selected for the measurements, employing a mass resolving power (MRP,  $m/\Delta m$ ) of 300 (Ag, Cd, Cu, Pb, Ti) or 4000 (Al, Fe, Si). A micro-droplet generator, MDG (Microdrop



Technologies, GmbH, Norderstedt, Germany) was used for droplet introduction. The instrumental setup was described previously in detail.

The nozzle diameter of the dispenser head was 50  $\mu\text{m}$  and the droplets were generated using triple pulse mode.<sup>24</sup> The droplet sizes were set as small as possible to minimize sample uptake and were in the range of 45–55  $\mu\text{m}$ , depending on daily tuning. The droplets were dispensed at a frequency of 100 Hz and He gas was introduced *via* the dispenser head to accelerate evaporation of the solvent.<sup>21</sup> The initial droplet diameters were continuously recorded with a CCD camera<sup>21–23,30,32</sup> during the measurements. The MDG adapter was attached directly to the ICP torch holder using a custom-made assembly, allowing that the entire setup can be moved together with the torch.<sup>30</sup> Droplet images were captured using Virtual Dub (V. 1.9.11, Avery Lee, Free Software Foundation Inc., Cambridge, USA) and their sizes were extracted using ImageJ (National of Health, Bethesda, MA, USA).<sup>33</sup> Argon was added as carrier gas to the droplet stream and mixed with either oxygen or nitrogen and introduced into a custom-made adapter that held the dispenser head. Standard Pt cones were used for experiments involving both oxygen and nitrogen, while a Ni “Jet” sampler and an “X” skimmer cones were used for experiments with the addition of nitrogen.

Data acquisition was carried out as described previously.<sup>30</sup> In Table 1 used acquisition and operating parameters of the ICPMS are listed. Transport efficiency (TE) was determined directly by recording the  $^{13}\text{C}^+$  ion signals and counting the number of events originating from the droplets and relating these to the total number of droplets produced by MDG during the measurement. The TE was checked at the beginning and end of each NP analysis. To increase the carbon signal to background ratio during these measurements, no nitrogen gas was added in this step. Daily optimization was carefully performed in order to achieve stable droplet trajectories while minimizing carbon molecular interferences and to avoid carbon deposition on the surfaces of the vacuum interface and cones. Daily optimization of the droplet introduction required certain adjustments of the carrier gas, which resulted in slight changes of the optimized sampling depth (Table 1).

The MDG operating parameters are listed in Table S1.†

For data evaluation, raw data were processed using custom written code for Matlab® (R2017b, MathWorks, Inc.) and further evaluation was performed using Excel® (Microsoft Corp.). After selecting a threshold value, at which the background originating from the sample could be separated from the NP signals, background subtraction was performed, and split correction was applied if the signal intensity of the subsequent data points was equal to or higher than the threshold. Background signals were usually obtained from the mean intensities observed when introducing the blank solvent. Depending on the operating conditions however,  $^{28}\text{Si}$  in toluene and  $^{49}\text{Ti}$  and  $^{63}\text{Cu}$  in mesitylene were eventually found to show distinct peaks in the transient signals, occurring at the frequency of the droplet introduction. In these cases the mean droplet signal was used for background subtraction.

At least 500 NP events were recorded per analysis. In order to determine the mass of investigated NPs, a standard solution

with dissolved Ti and Ag was used for calibration. The absolute sensitivity was determined from the dissolved concentration and the size of the droplets introduced into the ICP. The detection efficiency, which represents the number of ions detected per atoms present in a droplet, was calculated using eqn (1):

$$\text{DE} = \frac{M \times I \times 6 \times 10^{12}}{N_{\text{A}} \times A \times c \times d_{\text{drop}}^3 \times \pi} \quad (1)$$

where DE (ion counts per atoms) is the detection efficiency,  $M$  ( $\text{g mol}^{-1}$ ) is the molar mass of the analyte,  $I$  (ion counts) is the background corrected ion signal of the measured isotope per acquisition,  $N_{\text{A}}$  is Avogadro's number,  $A$  is the relative abundance of the isotope measured,  $c$  ( $\text{g mL}^{-1}$ ) is the concentration of the element in solution, and  $d_{\text{drop}}$  ( $\mu\text{m}$ ) is the diameter of the droplet introduced into the ICP *via* MDG.

Limits of detection (LODs) were estimated based on counting statistics,<sup>34</sup> therefore LOD based on mass is calculated according to eqn (2), while assuming a spherical shape of the NPs, LOD based on size is reported according to eqn (3):

$$\text{LOD}_{\text{mass}} = \frac{M \times (3.29 \times s_{\text{bg}} + 2.71)}{N_{\text{A}} \times A \times \text{DE}} \quad (2)$$

$$\text{LOD}_{\text{size}} = \sqrt[3]{\frac{6 \times \text{LOD}_{\text{mass}}}{\pi \times \rho_{\text{NP}} \times X_{\text{NP}}}} \quad (3)$$

where  $s_{\text{bg}}$  (counts) is the standard deviation of the background signal,  $\rho_{\text{NP}}$  ( $\text{g cm}^{-3}$ ) is the density of the NP and  $X_{\text{NP}}$  is the mass fraction of the element in the NP.

## Results and discussion

### Background signals and detection efficiency (DE)

**“Jet” interface.** By addition of nitrogen to the ICP when using the “Jet” interface, DEs of different elements increased when analysing aqueous suspensions<sup>30</sup> with MDG-based sample introduction. To investigate whether a similar improvement can be achieved with organic solvents, the same setup was employed. We selected 8 elements present in the multi-element standard to approximately cover the  $m/z$  range of atomic ions. Background signals and DE were determined for 13 isotopes of interest. Background signals were obtained by introducing blank toluene and mesitylene samples. For the latter, distinct transient peaks were observed for  $^{49}\text{Ti}$  and  $^{63}\text{Cu}$ , which occurred at the frequency of the droplet introduction, indicating either contamination or molecular ions formed from droplet residues. In these cases the actual droplet-related signals were used for background subtraction. DEs were determined by introduction of a standard of known concentration of the elements in toluene or mesitylene directly. Fig. 1 shows the signal intensities of the blank toluene sample as a function of nitrogen gas flow rate for the isotopes measured using an MRP of 300 (Ti, Cu, Ag, Cd, Pb) or 4000 (Al, Si, Fe). It can be seen that the background intensities increased with nitrogen addition, and peaked at flow rates between 10 and 15  $\text{mL min}^{-1}$ . A similar trend was observed for all elements except Al, where the background intensity



Table 1 ICPMS parameters

Acquisition parameters		Operating parameters	
Samples per peak	1000	Sampling depth, mm	−4.9–2
Sample (dwell) time, ms	1	Carrier gas, L min <sup>−1</sup>	1
Settling time, ms	1	Sample uptake, μL min <sup>−1</sup>	0.02–0.5
Mass window, %	5	Auxiliary gas, L min <sup>−1</sup>	1
Runs (NPs)	5000	RF power, W	1350
Runs (dissolved analytes)	500–1000	Nitrogen gas, mL min <sup>−1</sup>	0–20
Passes	1	Oxygen gas, mL min <sup>−1</sup>	0–15
Detection mode (standards and NPs)	Counting	Helium gas, L min <sup>−1</sup>	0.5–0.7
Detection mode ( <sup>13</sup> C)	Faraday		
# replicates (NPs)	3 (TiO <sub>2</sub> ); 5 (Ag)		
# replicates ( <sup>13</sup> C)	1		
Total acquisition time, s (NPs)	750 (Ti); 1250 (Ag)		
Total acquisition time, s (dissolved analytes)	25–50		
Mass resolving power, MRP	$m/\Delta m = 300$ : Ti, Cu, Ag, Cd, Pb		
	$m/\Delta m = 4000$ : Al, Si, Fe		

decreased steadily. It is important to note that the intensity ratios measured for different isotopes of Ti, Cu, Ag, and Cd were significantly offset from their respective natural abundance ratios, which indicates that molecular ions were formed upon introduction of the organic solvent. The intensity ratio <sup>208</sup>Pb/<sup>207</sup>Pb on the other hand was approximately 2, which could as well indicate Pb being present in the solvent. The background equivalent concentrations (BECs), estimated based on the sensitivities determined with the dissolved standard, amounted to less than 0.5 μg kg<sup>−1</sup> for Cu, Ag, Cd, and Pb and up to 3 μg kg<sup>−1</sup> for Ti.

The background signals for Al and Fe, measured in medium resolution, were close to the baseline noise with BECs of less than 0.05 μg kg<sup>−1</sup>, indicating that potentially occurring molecular ions were also resolved from the atomic ions. The background of <sup>28</sup>Si<sup>+</sup>, on the other hand, was substantial and corresponded to a BEC of 48 μg kg<sup>−1</sup>. Since the adjacent molecular ions (e.g. <sup>12</sup>C<sup>16</sup>O<sup>+</sup>, <sup>13</sup>C<sup>15</sup>N<sup>+</sup> and <sup>14</sup>N<sub>2</sub><sup>+</sup>, Fig. S2†) were mass-resolved, this is most likely due to a constant instrumental background.

The influence of nitrogen gas addition on the detection efficiencies (DEs) of the atomic ions is presented in Fig. 2. Similar to the background signals, the DEs first increased when nitrogen gas was added. The highest intensities were obtained at a nitrogen flow rate of 10 mL min<sup>−1</sup>, where DEs improved by up to 8 times, depending on the element. The least enhancement was obtained for Al and Fe by a factor of less than 2, whereas the DEs for Si, Ti, Cu, Ag and Cd increased by a factor of 3 to 5. The highest impact of nitrogen addition was observed for Pb, where the DE was higher by a factor of 8. Due to the low Si signal to background ratio however, nitrogen flow rates higher than 12 mL min<sup>−1</sup> did not yield a detectable signal anymore. DEs for the different isotopes of Ti, Cu, Ag, Cd and Pb showed good agreement, indicating that spectral interferences did not affect the analyses significantly. The experiments were repeated on another day and the results are shown in Fig. S3 and S4.† The data show the same general trends in the background signals and DEs in particular. While the background intensities for Ag, Cd, and Pb were essentially identical, Ti, Si and Al showed larger

deviations. DEs on the other hand were highly reproducible for Ag, while all other elements showed approximately 50% lower DEs on the second day. We assume that these deviations are also due to slightly different operating conditions used.

Similar experiments were carried out using mesitylene as solvent. The respective dependencies of the isotopes' background intensities and detection efficiencies on nitrogen flow rate with the "Jet" interface are presented in Fig. S5 and S6.† Background intensities were enhanced and peaked at nitrogen flow rates between 10 and 15 mL min<sup>−1</sup> for most isotopes measured, except for <sup>47</sup>Ti, <sup>27</sup>Al and <sup>56</sup>Fe. The background intensities from toluene and mesitylene were similar for Ag, Cd, Pb and Fe. Higher background signals occurred for Ti and Al in mesitylene, while Cu backgrounds were about 8–10 times lower. The highest DEs (Fig. S6†) were again obtained at a nitrogen flow rate of 10 mL min<sup>−1</sup>, resulting in a 5 to 8-fold improvement depending on the isotope. At a flow rate of 10 mL min<sup>−1</sup>, the BECs for Ag, Cd, Cu, Pb and Fe in mesitylene were less than 0.25 μg kg<sup>−1</sup>, while for Ti and Al up to 8 μg kg<sup>−1</sup> were observed.

**Standard interface.** Background signals and DEs were also determined using the standard interface using platinum sampler and skimmer cones, which also allowed for the addition of oxygen to the aerosol stream. While addition of nitrogen did not yield any improvement in terms of DE or background signal intensities, as exemplified for Pb in Fig. 3E and 4E, the addition of oxygen reduced the instrumental background signals in particular for <sup>47</sup>Ti, Cu, Ag and <sup>112</sup>Cd, Al and Fe. <sup>49</sup>Ti, <sup>111</sup>Cd and the Pb isotopes increased at 10 mL min<sup>−1</sup> oxygen flow rate and dropped slightly again when 15 mL min<sup>−1</sup> were used (Fig. 3). A dramatic increase in background signals for <sup>28</sup>Si upon addition of oxygen however prevented the use of this isotope in this study. Despite the reduction of the background signals, which supposedly is caused by the combustion of the organic molecular ions, the background signals remained either at a similar level (Ag) or higher than with the "Jet" interface and nitrogen addition, even at the highest oxygen flow rate.

In Fig. 4 the dependence of DE on different oxygen flow rates is presented, showing a steady decrease in DE with oxygen addition for all elements.



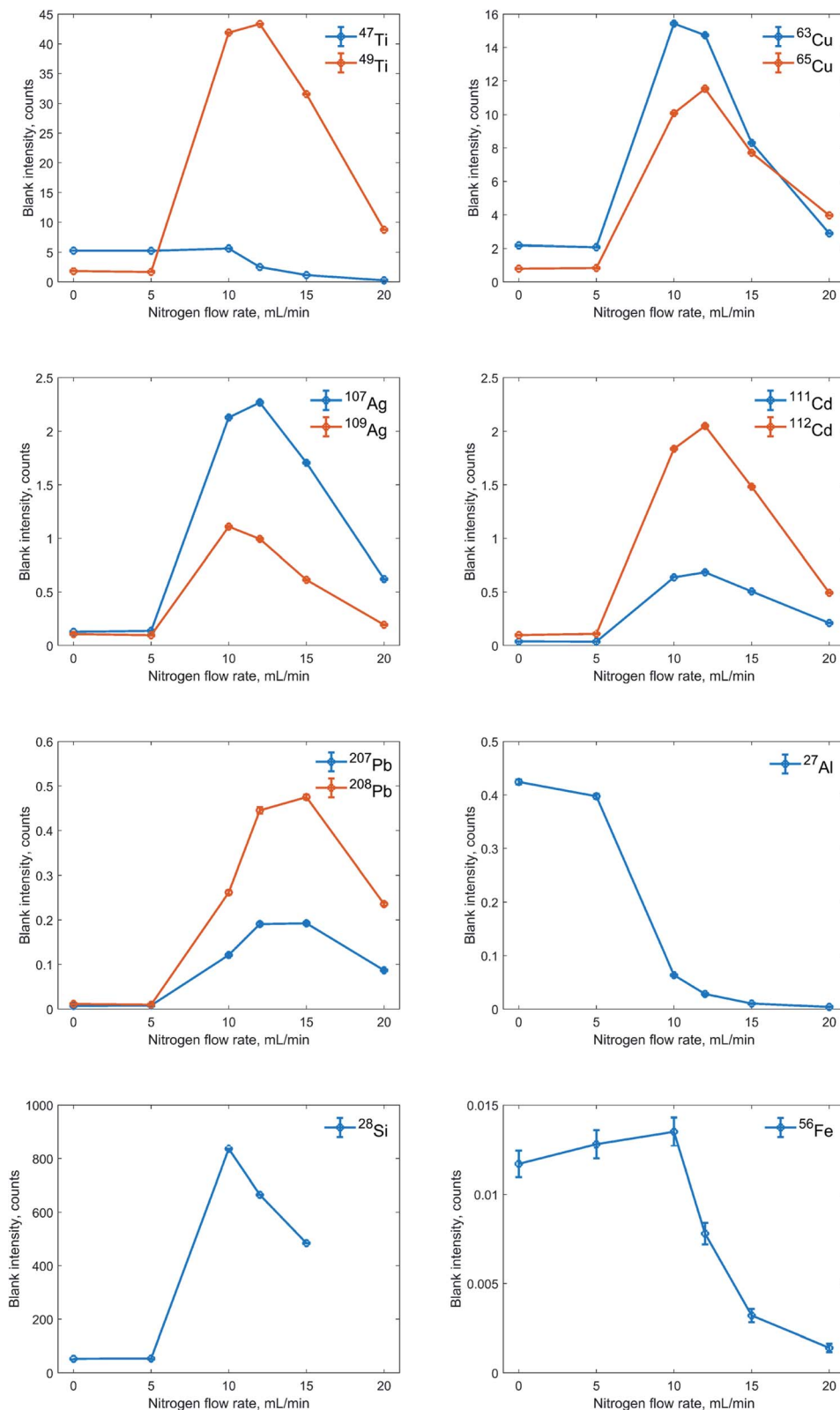


Fig. 1 Dependence of the isotopes' background intensities on the flow rate of nitrogen for toluene with the "Jet" interface. Error bars represent the standard error of 25 000 acquisitions.



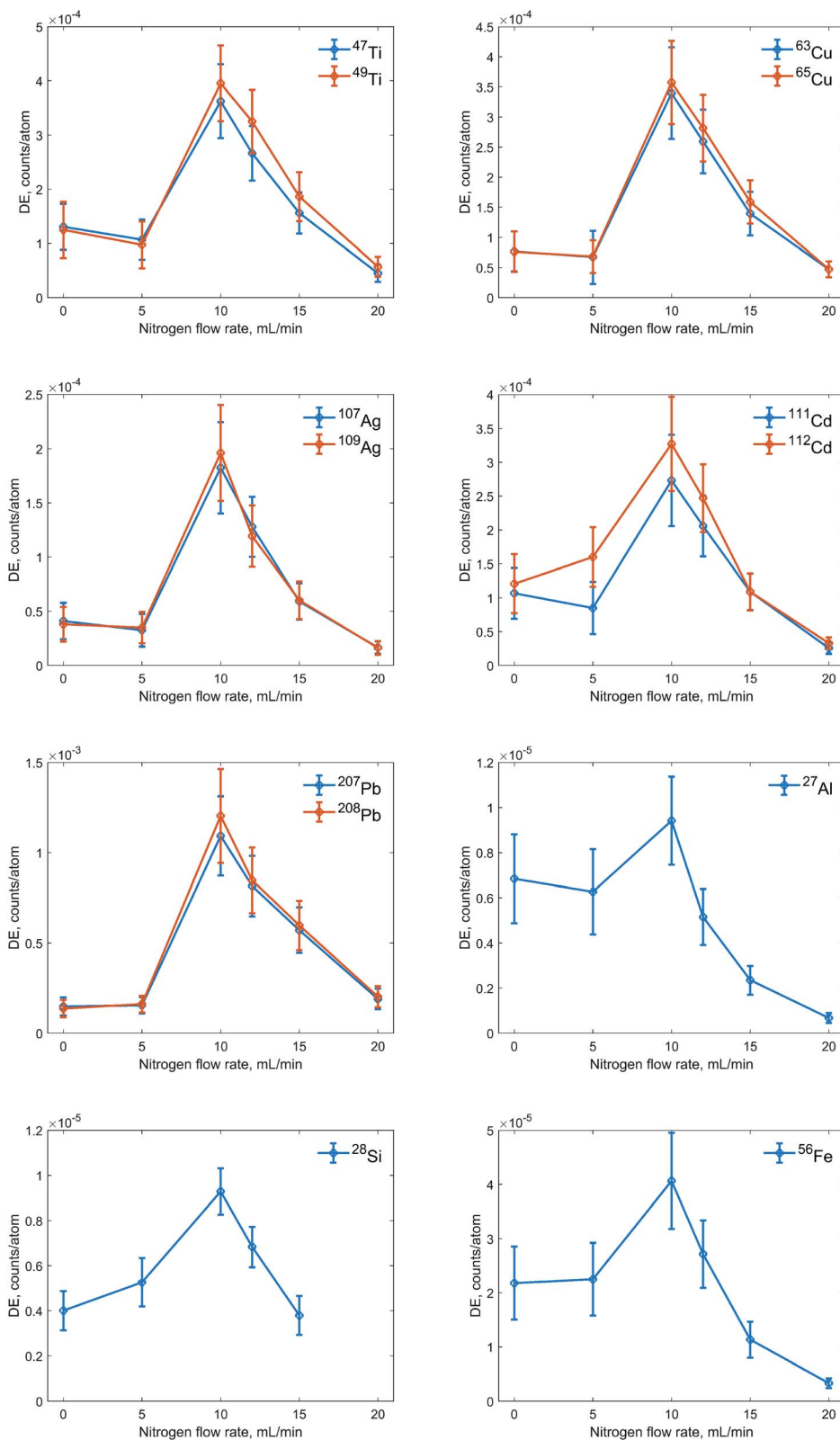


Fig. 2 Influence of nitrogen addition on the detection efficiency of 13 isotopes with the "Jet" interface. Error bars represent the standard deviation.



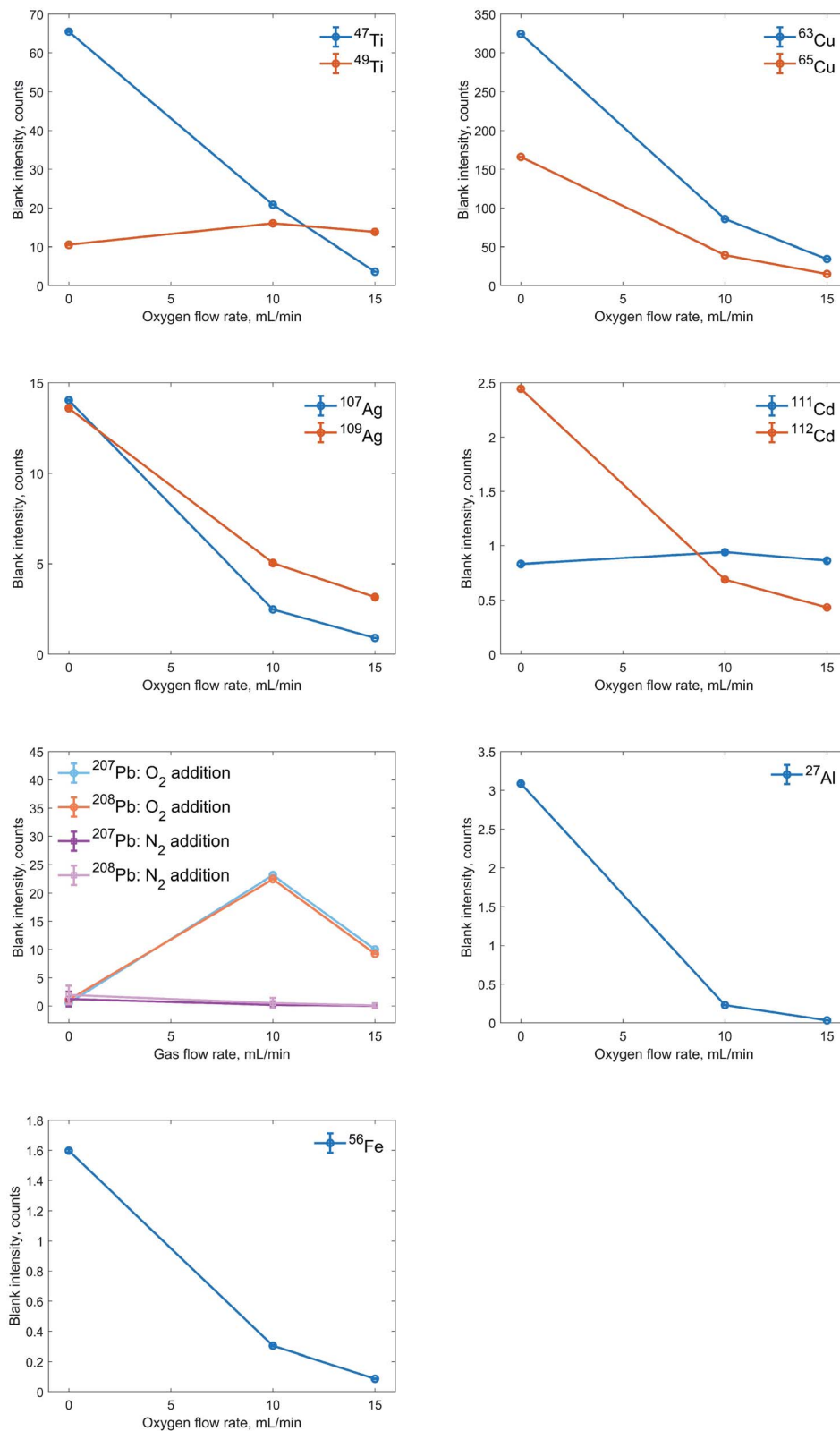


Fig. 3 Dependence of the isotopes' background intensities on the flow rate of oxygen for toluene, when using the standard interface. The error bars represent the standard error of 25 000 acquisitions.



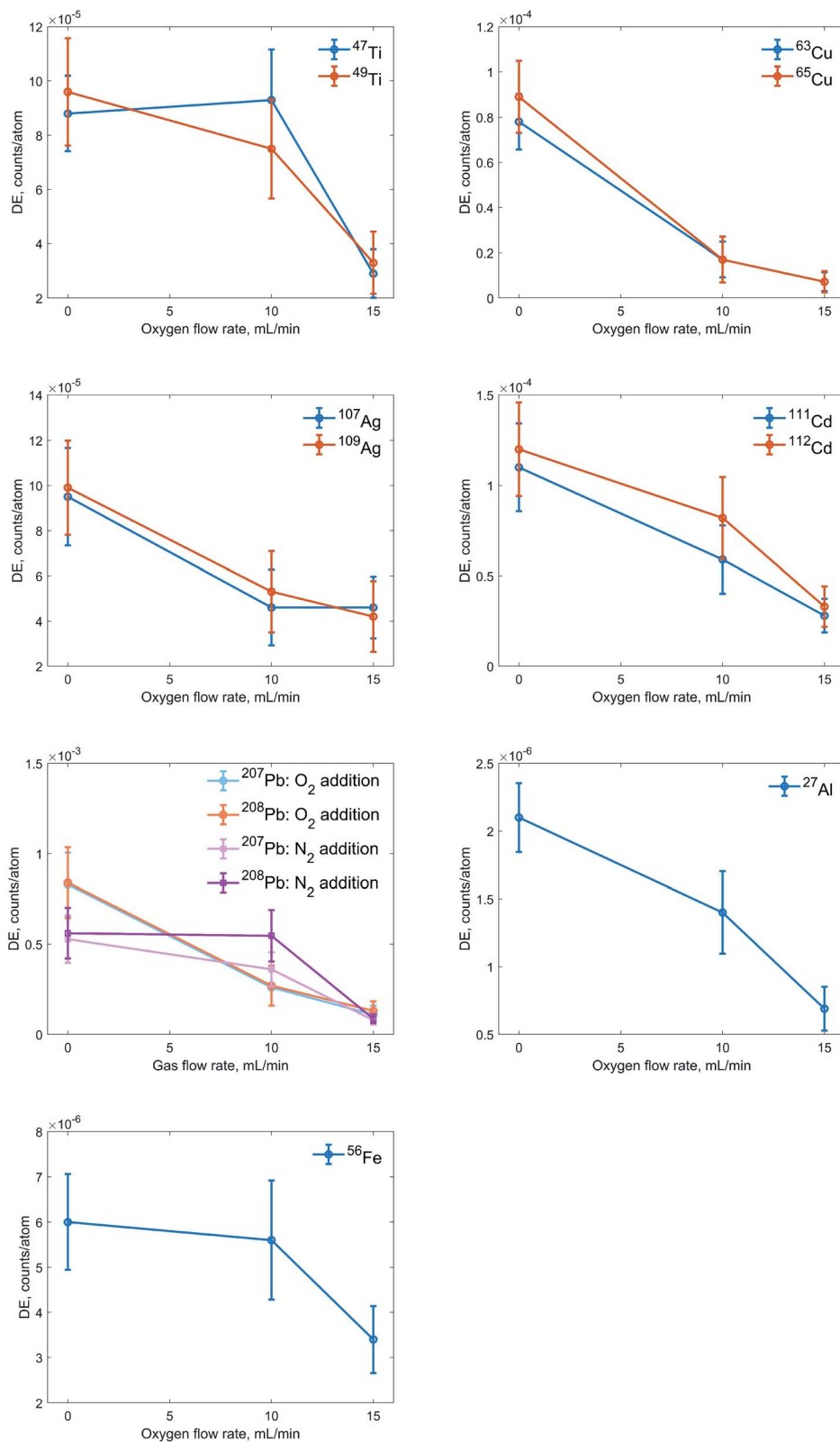


Fig. 4 Influence of oxygen addition on the detection efficiency of 13 isotopes in toluene with the standard interface. Error bars represent the standard deviation.



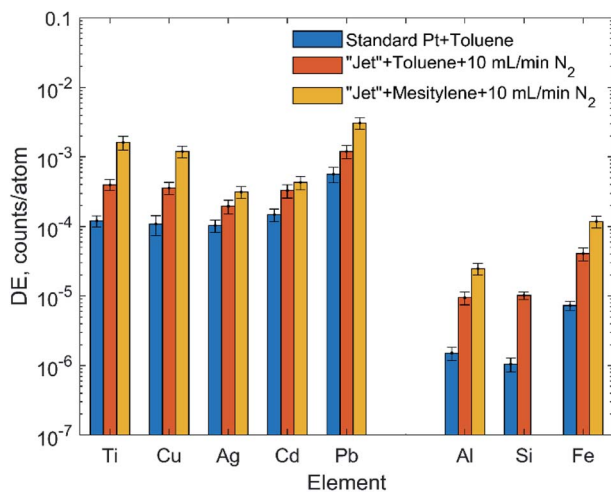


Fig. 5 Optimum DEs for 8 elements dissolved in toluene or mesitylene and measured in low (left part) and medium (right part) resolution. The data shown for the standard interface were obtained without gas addition, whereas for the experiments with "Jet" interface, the highest DE was obtained when using a nitrogen flow rate of 10 mL min<sup>-1</sup>.

### Detection efficiency (DE) and limit of detection (LOD)

As outlined before, the highest analyte sensitivity when using the "Jet" interface was obtained when adding 10 mL min<sup>-1</sup> N<sub>2</sub> to the aerosol flow. Using the standard interface, gas addition generally led to signal suppression. Thus, under optimized conditions, the "Jet" interface could improve the sensitivity by up to 8 times when compared to the standard configuration (Fig. 5) for elements dissolved in toluene. In mesitylene the DE could be improved by up to 4 times when compared to the

toluene solutions. Isotopes measured in low resolution yielded a DE of near 1‰ in the best case (Pb) while sensitivity naturally was lower by about an order of magnitude for elements measured at medium MRP.

The resulting LODs on the other hand did not only depend on the DE but were affected by the background signals too. The increase in background signals with nitrogen addition when using the "Jet" interface, more than compensated for by the higher DE for this configuration. Thus, the lowest limits of detection were obtained for a nitrogen flow rate of 10 mL min<sup>-1</sup> (Table 2). LODs for the standard interface were typically lowest without gas addition but between 2 and 20 times higher than for the "Jet" configuration. LODs for <sup>47</sup>Ti, <sup>107</sup>Ag, Al and <sup>56</sup>Fe could be slightly improved ( $\approx 30\%$ ) by adding oxygen to the ICP (Table 2). Using the "Jet" interface, single digit nm particle size LOD could be achieved for <sup>56</sup>Fe, <sup>63</sup>Cu and <sup>208</sup>Pb in this study. <sup>28</sup>Si and <sup>49</sup>Ti, which showed the highest background signals, on the other hand, were only detectable at levels higher than 100 ag or a particle size equivalent of several 10 nm. Despite the lower sensitivity by measuring in medium resolution, avoiding spectral overlaps could improve the detection capabilities as exemplified by <sup>56</sup>Fe, where a mass LOD of 3 ag or a size LOD of 9.2 nm could be achieved. It is also apparent that the improvement in LOD when using the "Jet" interface was again more pronounced for lighter isotopes like it was the case with aqueous droplets as previously observed.<sup>30</sup>

### Nanoparticle analysis

**Ag NPs in toluene.** In order to verify whether NP mass and size can also be quantified using dissolved standards solutions, citrate-based Ag NPs of known size (manufacturer: 78.9  $\pm$

Table 2 Background signal intensity (Bg), sensitivities (S) and resulting mass LOD (LODm) and size LOD (LODs) for 13 isotopes measured using standard and "Jet" cones under optimized conditions

Element	Ti		Cu		Ag		Cd		Pb		Al	Si	Fe
Isotope	47	49	63	65	107	109	111	112	207	208	27	28	56
MRP	300						4000						
<b>Standard interface, toluene, no gas or optimum O<sub>2</sub> flow rate</b>													
S [cts ag <sup>-1</sup> ]	0.03 <sup>e</sup>	0.06	0.52	0.26	0.13 <sup>e</sup>	0.27	0.75	0.15	0.53	1.3	0.03 <sup>d</sup>	0.03	0.06 <sup>d</sup>
Bg, cts <sup>a</sup>	4 <sup>e</sup>	11	324	166	1 <sup>e</sup>	14	1	2	0.5	1	0.2 <sup>d</sup>	56	0.3 <sup>d</sup>
LODm, ag	380 <sup>e</sup>	710	210	250	50 <sup>e</sup>	110	130	62	11	5.3	140 <sup>d</sup>	1240	86 <sup>d</sup>
LODs, nm <sup>b</sup>	55 <sup>e</sup>	67	36	38	21 <sup>e</sup>	27	30	24	12	9.6	47 <sup>d</sup>	100	28 <sup>d</sup>
<b>"Jet" interface, toluene, 10 mL min<sup>-1</sup> N<sub>2</sub></b>													
S [cts ag <sup>-1</sup> ]	0.35	0.26	2.3	1	0.53	0.52	0.19	0.43	0.7	1.83	0.21	0.18 (0.15 <sup>c</sup> )	0.4
Bg, cts <sup>a</sup>	6	42	15	10	2.1	1.1	0.6	1.8	0.1	0.3	0.1	840 (60 <sup>c</sup> )	0.01
LODm, ag	33	120	17	23	16	13	30	18	5.9	2.9	17	1370 (290 <sup>c</sup> )	7.8
LODs, nm <sup>b</sup>	24	37	15	17	14	13	19	16	10	7.8	23	104 (62 <sup>c</sup> )	12
<b>"Jet" interface, mesitylene, 10 mL min<sup>-1</sup> N<sub>2</sub></b>													
S [cts ag <sup>-1</sup> ]	1.2	1.04	6.46	3.44	0.85	0.83	0.22	0.56	1.97	4.11	0.55		1.17
Bg, cts <sup>a</sup>	77	58	10	1.4	0.9	0.8	0.1	0.3	0.1	0.2	3.1		0.1
LODm, ag	33	49	2.3	2.7	18	15	18	10	2.2	1.4	17		3.2
LODs, nm <sup>b</sup>	24	28	7.8	8.3	15	14	16	13	7.2	6.1	23		9.2

<sup>a</sup> Mean counts per acquisition of 1 ms. <sup>b</sup> Corresponding to the element. <sup>c</sup> Data obtained at 6 mL min<sup>-1</sup> N<sub>2</sub>. <sup>d</sup> Data obtained at 10 mL min<sup>-1</sup> O<sub>2</sub>. <sup>e</sup> Data obtained at 15 mL min<sup>-1</sup> O<sub>2</sub>.



3.9 nm, measured:  $79.5 \pm 3.9$  nm) were solvent exchanged and suspended in toluene. High angular annular dark field (HAADF-STEM) images of these NPs before and after the solvent exchange are shown in Fig. S7.† After the solvent exchange, the NPs deposited on the TEM grid were found to occur as loosely bound agglomerates of several 100 particles after evaporation of the solvent, which made an automated size evaluation difficult. Upon visual assessment, however, the particle sizes do not appear substantially altered by the solvent exchange. For the sp-ICPMS analyses, the optimized conditions with the “Jet” interface were employed. However, after considering the NP mass and DE for Ag in this configuration, it turned out that the signal intensities would reach the upper limit of the linear dynamic range of the counting detection mode. Therefore, the sensitivity was attenuated by a factor of 15 by defocusing the ion beam in the ion optics of the ICPMS. Thus, both, the NP suspension and the dissolved standard, were measured under defocused ion beam conditions. For calibration, the Conostan S21 reference standard, diluted in toluene to a concentration of  $12 \mu\text{g kg}^{-1}$  Ag, was introduced as droplets of approx. 50  $\mu\text{m}$  in diameter directly into the ICP. In this way, the absolute sensitivity was determined and, assuming spherical shape of the NPs, their size was calculated. In Fig. 6 the resulting signal intensity (left) and size distribution (right) histograms are shown. The particle size mode diameter was determined as  $84.8 \pm 17.7$  nm, which is in reasonable agreement to the reference value. Mean and median diameters were found to be 95.8 nm and 87.9 nm, respectively, *i.e.* larger than the reference value. This deviation is most likely caused by a substantial number of multiple NPs events recorded during the acquisition. As shown in Fig. 6, the single particles' signal mode was found near 200 cts while an additional mode appeared near 400 cts, which most likely results from 2 particles detected per droplet. Since the number of detected events,  $<10^3$  from  $10^5$  individual droplets, was sufficiently small to avoid such a high fraction of individual particles being present in a single droplet, we consider these to be aggregates that formed already before the droplet formation.

Particle aggregation is further corroborated by the fact that the number of detected events dropped continuously during the analysis. Within 20 minutes of measurement the number of registered particle events fell to about 10% of the initial count (Fig. S8†). The transport efficiency, as determined by the  $^{13}\text{C}$  signal (Fig. S9†) at the beginning and the end of the sequence, on the other hand remained constant during the analysis, indicating that droplet injection was stable. After loading a freshly sonicated sample into the MDG however, the initial particle count could be restored. These observations would indicate that these metallic NPs, when suspended in toluene, aggregate or sediment fairly rapidly. An accurate particle number determination is thus not possible under these conditions and would require a more effective stabilization of such NP suspensions. The NP size determination on the other hand appears to be readily possible, when considering the good agreement of the NP mode size.

**TiO<sub>2</sub> NPs in sunscreens.** Two different brands of sunscreen, containing TiO<sub>2</sub> NPs as UV-absorbent, hereafter referred to as “A” and “B”, were analysed by the same approach as outlined above. They were dissolved directly in toluene with a dilution factor of  $\sim 10^6$ . Calibration of the absolute sensitivity was again carried out using the Conostan S21 multi-element standard diluted in toluene and using  $^{47}\text{Ti}$  as the more sensitive isotope. Prior to sample analysis, a toluene blank sample was measured to assess the background intensity of Ti and verify the absence of Ti-containing nanoparticles in the system. The TE was again determined using  $^{13}\text{C}$  as droplet tracer at the beginning and the end of each sequence and was found to be 98.9% and 98.8% for samples “A” and “B”, respectively. It should be noted here that the efficiency of droplet transfer is actually 100% and that the deviation is simply because a fraction of droplets arrived in the ICP during the “flyback” time of the MS. Yet the PNCs were corrected for the missed droplets. NP data were collected for both sunscreen samples and are shown in Fig. 7. As already observed for the Ag NPs, the number of registered particle events dropped substantially over the course of the

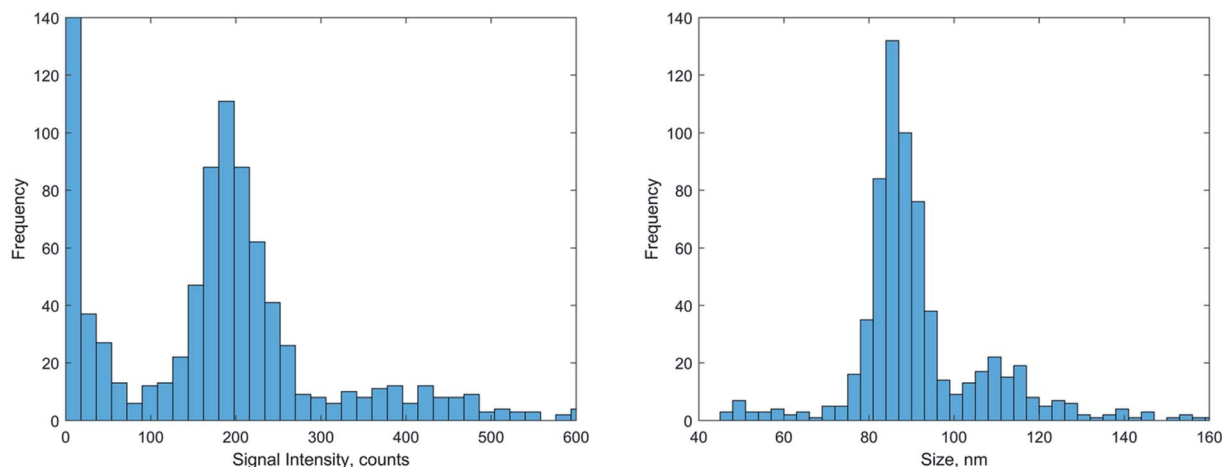


Fig. 6 The sp-ICPMS measurement of 80 nm Ag NPs suspended in toluene. The signal intensity distribution (left) and size distribution (right) histograms.



measurement (Fig. 7 left). In both samples the particle events decreased by almost 70% towards the end of the analysis, again hampering assessment of the particle number concentration. If only the particle counts within the first 4 minutes of the experiment were used for the calculation of the particle number concentration, it would result in  $3.7 \times 10^{11} \text{ g}^{-1}$  for sample "A" and  $5.9 \times 10^{11} \text{ g}^{-1}$  for sample "B" when diluted in toluene only. The mass fractions of  $\text{TiO}_2$  in the sunscreens would thus correspond to  $0.15 \text{ mg g}^{-1} \text{ TiO}_2$  in sample "A" and  $0.29 \text{ mg g}^{-1} \text{ TiO}_2$  in sample "B", which corresponds to only 0.4% of the  $\text{TiO}_2$  present in the original sample, as determined after digestion. This low recovery indicates that the major fraction of  $\text{TiO}_2$  NPs had settled and/or aggregated from the toluene before the analysis. The intensity histograms (Fig. 7 left) are characterized by more or less continuous distributions above the instrumental background, whose shape did not vary appreciably over time. However, in particular sample "B" seems to show a multimodal distribution which is most likely caused by the NP aggregates formed as discussed before. The resulting size distributions are thus very broad for both samples spanning a size range of 34–136 nm and 34–100 nm  $\text{TiO}_2$  NPs for samples "A" and "B", respectively (Fig. 7 right).

To evaluate the stabilisation efficiency of different solvents, mesitylene and diphenyl ether were studied for their higher

viscosities (toluene:  $0.59 \text{ mPa s}$  at  $20^\circ \text{C}$ , mesitylene:  $0.83 \text{ mPa s}$  at  $20^\circ \text{C}$ , diphenyl ether:  $3.3 \text{ mPa s}$  at  $30^\circ \text{C}$ ). The generation of droplets was however not successful with diphenyl ether, while stable droplets could be reproducibly formed from mesitylene. Furthermore, it was tested if the addition of 10 mM dodecanethiol (DDT) to the organic solvents might reduce agglomeration of the NPs. Finally, the PNC data were also compared to an aqueous suspensions, prepared according to a protocol described previously.<sup>31</sup> Here, only sunscreen "B" was analysed after dilution by  $\sim 10^5$  (water),  $\sim 5.5 \times 10^6$  (mesitylene),  $\sim 3.5 \times 10^6$  (toluene). Fig. 8 shows the PNCs and their variation over three replicates for the different solvents. The mean PNCs obtained varied substantially between  $2.24 \times 10^{11} \text{ g}^{-1}$  (water) and  $2.85 \times 10^{13} \text{ g}^{-1}$  (toluene with 10 mM DDT). As was observed before, the PNCs measured in toluene without DDT dropped by about 60–70% over the course of 3 replicates or 12 minutes of analysis. The addition of DDT not only caused the PNC to increase by more than an order of magnitude but also reduced the drop-in particle events during the analyses. PNCs measured in mesitylene on the other hand appeared more reproducible during the analyses and the addition of DDT did not cause substantial changes in the measured PNC. The aqueous suspension also appeared to be comparably stable over the course of the analyses but PNCs were by more than an order of

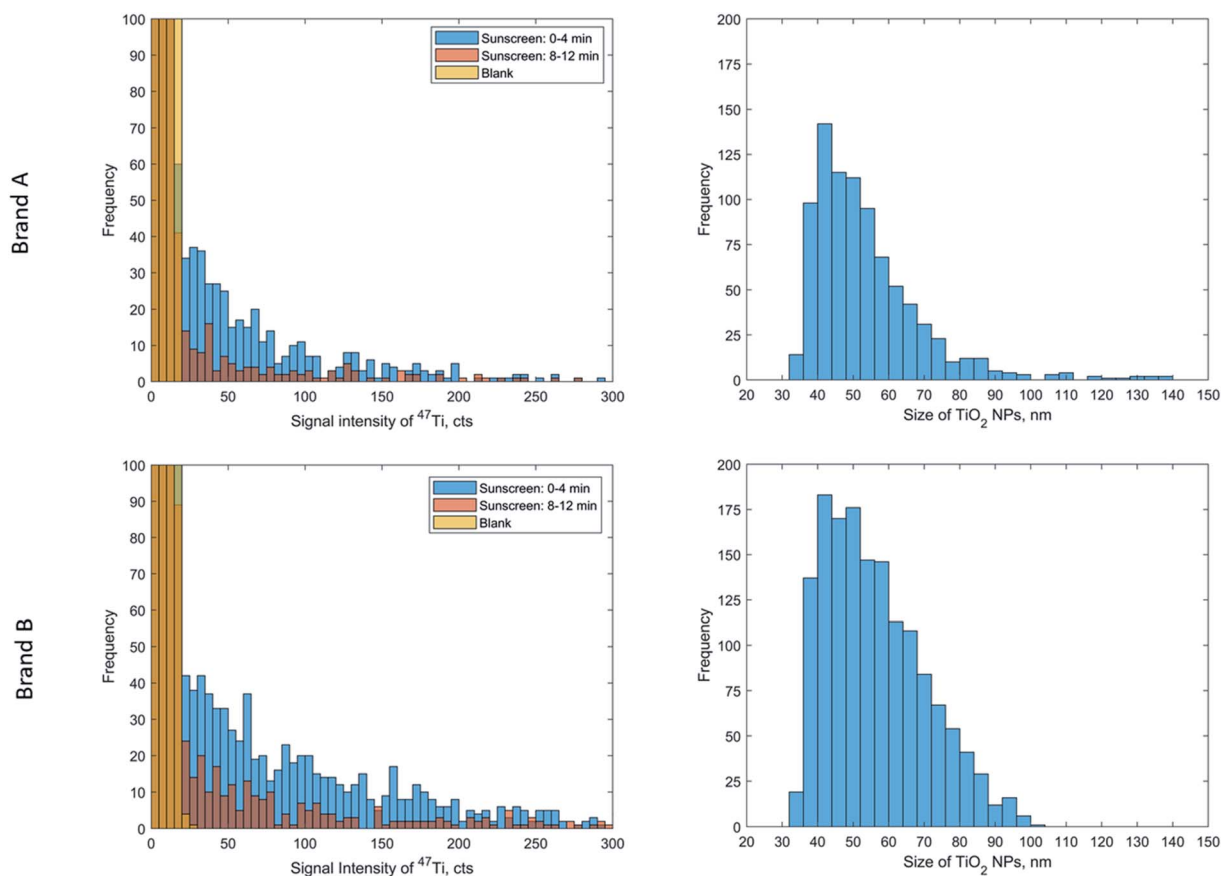


Fig. 7 Data set acquired for sunscreen samples diluted in toluene. Top and bottom panels correspond to sunscreen samples "A" and "B", respectively. Left: signal intensity histograms showing the toluene blank (orange) and results for the sunscreen samples at the beginning (0–4 min, blue) and the end (8–12 min, red) of the measurement sequence; right: particle size distribution from the entire dataset for each sample.



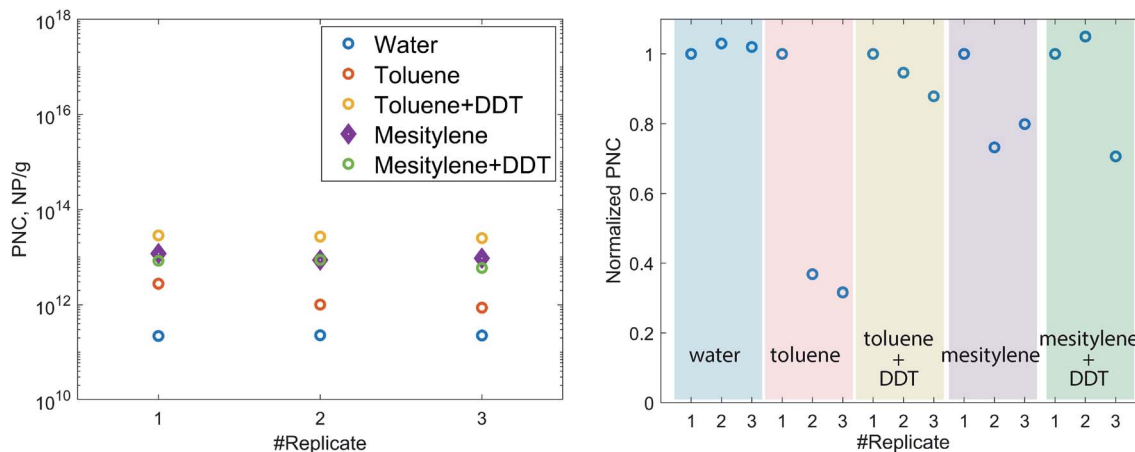


Fig. 8 Comparison of calculated  $\text{TiO}_2$  PNC according to the solvents used for dilutions of sunscreen "B" (left) and normalized  $\text{TiO}_2$  PNC to the replicate #1 for respected solvent (right). One replicate is equal to 4 min 16 s measurement time.

magnitude lower than for the organic suspensions. The PNCs, particle sizes and experimental sensitivities and background signals for these analyses are compiled in Table S2.† It also contains the NP mass fraction determined in the sunscreen, determined from the initial PNC and assuming that the measured sizes correspond to compact single NPs. It was in all cases only a small fraction of the total determined after sunscreen digestion and conventional analysis by ICPMS. This would indicate that the majority of the  $\text{TiO}_2$  NPs could not be suspended in any of the solvents in these experiments. It is most likely that the NPs either undergo a rapid agglomeration during sample preparation or are already present as agglomerates in the sunscreen itself. Such aggregates were actually observed by scanning transmission electron microscopy after evaporation of the solvent (Fig. S10†).

## Conclusions

A microdroplet-based sample introduction setup was successfully applied to directly analyse organic solutions and suspensions by ICPMS. The low sample uptake effectively mitigated instrument drift, otherwise caused by soot deposition at the vacuum interface, and thereby allowed for stable, continuous operation. This approach can thus be used to determine the element content of samples that are either difficult to transfer into or not stable within aqueous solutions or suspensions. With the use of a "Jet" interface and the addition of  $10 \text{ mL min}^{-1}$  of nitrogen gas, the sensitivity of the elements studied could be improved by up to 8 times, when compared to operation with the conventional interface. It is expected that a similar improvement is attainable for other elements of interest. Molecular ions from the solvent were found to be still present in the mass spectra, and they do affect the attainable limits of detection when using an MRP of 300. At an MRP of 4000 on the other hand spectral interferences were substantially reduced for example for  $^{27}\text{Al}$  and  $^{56}\text{Fe}$ . Yet the BEC even for isotopes measured at low MRP were mostly in the low  $\mu\text{g kg}^{-1}$  range, which would still allow for trace element determinations

in organic solvents. With optimized conditions, LODs in the single-digit attogram range were obtained for Cu, Pb and Fe. Except for Si, the remaining elements studied had mass-LODs between 10 ag and 30 ag. For the conventional vacuum interface, also the addition of oxygen was studied and was effective in reducing the background signals from molecular ions. The reduction of the detection efficiency of the elements upon the addition of nitrogen or oxygen, however, prevented improving the limits of detection for most isotopes studied. The corresponding size LODs for NPs were thus lower by approximately two times with the "Jet" interface with nitrogen addition compared to the standard interface setup. Under these conditions, the determination of nanoparticle sizes could be successfully carried out for  $\text{TiO}_2$  and metallic Ag nanoparticles (mode diameter is in agreement with the manufacturer's specified NPs diameter), while accurate determination of particle number concentration was hampered by a rapid aggregation and settling of the NPs in toluene. In this solvent, the occurrence of particle events was found to continuously drop by 70% or 90% during a measurement sequence of only 12 minutes. Resonication of the samples restored the original events frequency, which suggests that the particles settle in the sample vial, and likely also on the inner surfaces of the transfer tubing or droplet generator. The addition of DDT had a positive effect on stabilization of the NP detection and recovery but the mass of titania NPs in a sunscreen sample could only be recovered to less than 4% of the total. We assume that the majority of the NPs either aggregate and settle very rapidly during sample preparation or are already present as too large aggregates in the original sample. Suspensions of these NPs in mesitylene exhibited did appear to be more stable over the course of an analysis which may be a result of its higher viscosity.

Nonetheless this approach appears to be a promising alternative to analysing the element content of organic media without the drawbacks encountered by ICPMS with spray chamber, where the addition of oxygen is required, which typically causes a significant signal suppression.



## Conflicts of interest

There are no conflicts to declare.

## Acknowledgements

This work was carried out in the frame of the Horizon 2020 funded project ACEnano *via* SBFI Ref-1131-52302 and supported by ETH Zurich.

## References

- 1 M. D. Montaña, J. W. Olesik, A. G. Barber, K. Challis and J. F. Ranville, *Anal. Bioanal. Chem.*, 2016, **408**, 5053–5074.
- 2 L. Hendriks, B. Ramkorun-Schmidt, A. Gundlach-Graham, J. Koch, R. N. Grass, N. Jakubowski and D. Günther, *J. Anal. At. Spectrom.*, 2019, **34**, 716–728.
- 3 R. M. Dragoman, M. Grogg, M. I. Bodnarchuk, P. Tiefenboeck, D. Hilvert, D. N. Dirin and M. V. Kovalenko, *Chem. Mater.*, 2017, **29**, 9416–9428.
- 4 Y. Kelestemur, Y. Shynkarenko, M. Anni, S. Yakunin, M. L. De Giorgi and M. V. Kovalenko, *ACS Nano*, 2019, **13**, 13899–13909.
- 5 S. F. Solari, S. Kumar, J. Jagielski, N. M. Kubo, F. Krumeich and C. J. Shih, *J. Mater. Chem. C*, 2021, **9**, 5771–5778.
- 6 F. Krieg, Q. K. Ong, M. Burian, G. Raino, D. Naumenko, H. Amenitsch, A. Süess, M. Grotevent, F. Krumeich, M. I. Bodnarchuk, I. Shorubalko, F. Stellacci and M. V. Kovalenko, *J. Am. Chem. Soc.*, 2020, **141**, 19839–19849.
- 7 M. J. Kim, H.-J. Na, K. C. Lee, E. A. Yoo and M. Lee, *J. Mater. Chem.*, 2003, **13**, 1789–1792.
- 8 N. Nakayama and T. Hayashi, *Colloids Surf., A*, 2008, **317**, 543–550.
- 9 A. B. Serrano-Montes, D. Jimenez de Aberasturi, J. Langer, J. J. Giner-Casares, L. Scarabelli, A. Herrero and L. M. Liz-Marzán, *Langmuir*, 2015, **31**, 9205–9213.
- 10 J. Nelson, M. Yamanaka, F. Lopez-Linares, L. Poirier and E. Rogel, *Energy Fuels*, 2017, **31**, 11971–11976.
- 11 J. Nelson, A. Saunders, L. Poirier, E. Rogel, C. Ovalles, T. Rea and F. Lopez-Linares, *J. Nanopart. Res.*, 2020, **22**, 304.
- 12 D. Ruhland, K. Nwoko, M. Perez, J. Feldmann and E. M. Krupp, *Anal. Chem.*, 2019, **91**, 1164–1170.
- 13 A. Leclercq, A. Nonell, J. L. Todolí, C. Bresson, L. Vio, T. Vercouter and F. Chartier, *Anal. Chim. Acta*, 2015, **885**, 57–91.
- 14 A. Leclercq, A. Nonell, J. L. Todolí, C. Bresson, L. Vio, T. Vercouter and F. Chartier, *Anal. Chim. Acta*, 2015, **885**, 33–56.
- 15 C. Agatemor and D. Beauchemin, *Anal. Chim. Acta*, 2011, **706**, 66–83.
- 16 C. S. K. Raju, L. L. Yu, J. E. Schiel and S. E. Long, *J. Anal. At. Spectrom.*, 2013, **28**, 901–907.
- 17 A. C. Lazar and P. B. Farnsworth, *Anal. Chem.*, 1997, **69**, 3921–3929.
- 18 R. N. Easter, K. K. Kröning, A. Caruso and P. A. Limbach, *Analyst*, 2010, **10**, 2560–2565.
- 19 R. Sánchez, J. L. Todoli, C. P. Lienemann and J. Mermet, *Spectrochim. Acta, Part B*, 2013, **88**, 104–126.
- 20 P. E. Verboket, O. Borovinskaya, N. Meyer, D. Günther and P. S. Dittrich, *Anal. Chem.*, 2014, **86**, 6012–6018.
- 21 J. Koch, L. Flamigni, S. Gschwind, S. Allner, H. Longenrich and D. Günther, *J. Anal. At. Spectrom.*, 2013, **28**, 1707–1717.
- 22 S. Gschwind, H. Hagendorfer, D. A. Frick and D. Günther, *Anal. Chem.*, 2013, **85**, 5875–5883.
- 23 S. Gschwind, L. Flamigni, J. Koch, O. Borovinskaya, S. Groh, K. Niemax and D. Günther, *J. Anal. At. Spectrom.*, 2011, **26**, 1166.
- 24 K. Shigeta, H. Traub, U. Panne, A. Okino, L. Rottmann and N. Jakubowski, *J. Anal. At. Spectrom.*, 2013, **28**, 646.
- 25 B. Ramkorun-Schmidt, S. A. Pergantis, D. Esteban-Fernández, N. Jakubowski and D. Günther, *Anal. Chem.*, 2015, **87**, 8687–8694.
- 26 L. Hendriks, A. Gundlach-Graham and D. Günther, *Chimia*, 2018, **72**, 221–226.
- 27 K. Mehrabi, A. Gundlach-Graham, D. Günther and A. Gundlach-Graham, *Environ. Sci.: Nano*, 2019, **6**, 3349–3358.
- 28 K. Shigeta, G. Koellensperger, E. Rampler, H. Traub, L. Rottmann, U. Panne, A. Okino and N. Jakubowski, *J. Anal. At. Spectrom.*, 2013, **28**, 637.
- 29 T. Vonderach, B. Hattendorf and D. Günther, *Anal. Chem.*, 2021, **93**, 1001–1008.
- 30 J. Kocic, D. Günther and B. Hattendorf, *J. Anal. At. Spectrom.*, 2021, **36**, 233–242.
- 31 R. Peters, I. Elbers, A. Undas, E. Sijtsma, S. Briffa, P. Carnell-Morris, A. Siupa, T. Yoon, L. Burr, D. Schmid, J. Tentschert, Y. Hachenberger, H. Jungnickel, A. Luch, F. Meier, J. Radnik, V. Hodoroaba, I. Lynch and E. Valsami-Jones, *Molecules*, 2021, **26**, 5315.
- 32 K. Shigeta, H. Traub, U. Panne, A. Okino, L. Rottmann and N. Jakubowski, *J. Anal. At. Spectrom.*, 2013, **28**, 646.
- 33 U. W. S. Rasband, *ImageJ*, U.S. National of Health, Bethesda, MA, <https://imagej.nih.gov/ij/>.
- 34 L. A. Currie, *Anal. Chim. Acta*, 1999, **391**, 105–126.

